Journal of Photochemistry and Photobiology A: Chemistry 232 (2012) 14–21

Contents lists available at SciVerse ScienceDirect

Journal of Photochemistry and Photobiology A: Chemistry

journal homepage: www.elsevier.com/locate/jphotochem

Chemical determination of singlet oxygen from photosensitizers illuminated with LED: New calculation methodology considering the influence of photobleaching

Adriana Passarella Gerola, Juliana Semensato, Diogo Silva Pellosi, Vagner Roberto Batistela, Bruno Ribeiro Rabello, Noboru Hioka, Wilker Caetano*

Chemistry Department, State University of Maringá, Brazil

ARTICLE INFO

Article history:
Received 22 June 2011
Received in revised form 17 January 2012
Accepted 21 January 2012
Available online 1 February 2012

Keywords:
Singlet oxygen
Uric acid
Photodynamic activity
LED
Photobleaching
Absorbed photon

ABSTRACT

The singlet oxygen ($^1O_2$) is one of the reactive species responsible for the destruction of target cells in Photodynamic Therapy (PDT). However, the quantification of $^1O_2$ yields (Φ_Δ) involves lifetime measurements with very expensive equipment. An alternative methodology is the use of a chemical trap, in the present case uric acid (UA), which promptly reacts with $^1O_2$ providing the evaluation of Φ_Δ. On the other hand, in the quantification of the photons absorbed by the PS employing LED as irradiation sources in this kind of experiments, it is important to evaluate the overlap of the light source in the PS spectrum. Additionally, while some PS are photostable, others may undergo photobleaching leading the amount of absorbed photons to vary with the illumination time due to PS degradation. The proposed methodology corrects this problem. The proposed dosimetry method employing UA and the absorbed photon calculations taking into account chlorophyll and xanthene dyes photobleaching resulted in Φ_Δ values that agree with the literature.

1. Introduction

The interaction of electromagnetic radiation with matter is the basis of the photochemical processes that occur after photon absorption by photoactive molecules and the promotion of electrons from the ground to an excited state [1]. The activation of a photosensitizer compound (PS) by radiation of appropriate wavelength [2] has been applied in Photodynamic Therapy (PDT) to treat diseases characterized by uncontrolled cell growth, such as cancer. These photochemical processes are also responsible for the photodynamic inactivation of microorganisms (PDI). The success of both techniques, PDT and PDI, is dependent on several factors, particularly on the ability of absorption of electromagnetic radiation by the PS and the light source emission in a given spectral range; both factors affect the spectral overlap between the PS absorption and the light source emission. However, many of the studied PS are unstable against light, which alters their ability to absorb light during illumination, resulting in a decreased efficiency of production of excited molecules [3]. The mechanism of action of PDT and PDI can follow two paths, type I and II, respectively. The type I mechanism involves the formation of reactive radical species, whereas the type II mechanism involves the formation of singlet oxygen ($^1O_2$), which is assumed as the main PDT mechanism. $^1O_2$ is a highly reactive species, and it is responsible for the destruction of target cells [4].

Singlet oxygen, the excited state of molecular oxygen, has the electrons paired in the valence shell and presents two forms with distinct symmetries, a low energy $^1\Delta_g$ doubly degenerate (two equivalent configurations, $^1\Delta_x$ and $^1\Delta_y$; 92.4 kJ mol^{-1}), and a second state with high energy ($^1\Sigma$; 159.6 kJ mol^{-1}). This second excited state of oxygen has a too short lifetime, since the transition to the state $^1\Delta_g$ is allowed by spin or the transition to the ground state $^3\Sigma_g$ is allowed by orbital symmetry. However, the different symmetry of the specie $^1\Delta_g$, when compared with the ground state $^3\Sigma_g$, and the spin transition prohibition of $^1\Delta_g$ to $^3\Sigma_g$, ensure that the specie $^1\Delta_g$ will have a lifetime that is long enough to allow the oxidation of biological substrates [5]. Most of the substrates are found as a singlet in the ground state, thus they do not readily react with triplet molecular oxygen due to the spin prohibition. Nevertheless, for the singlet oxygen this restriction is broken, providing greater reactivity. Additionally, the molecular orbital gap in the $^1\Delta_g$ state increases the electrophilic character of oxygen and its oxidant performance, attacking substrates containing sites with high electron density, such as unsaturated lipids, proteins, and nucleic acids with double bonds [5,6].

Among the methods of determination of quantum yield of singlet oxygen (Φ_Δ), time-resolved devices provide a direct quantification through the measurement of its phosphorescence lifetime (τ) at 1270 nm. Although the intensity of $^1O_2$ phosphorescence is

* Corresponding author at: Av. Colombo, 5790, Z07 – Maringá, 87020-900, Paraná, Brazil. Tel.: +55 44 3011 3665; fax: +55 44 3011 4125.
E-mail address: wcaetano@uem.br (W. Caetano).

1010-6030/$ – see front matter © 2012 Elsevier B.V. All rights reserved.
doi:10.1016/j.jphotochem.2012.01.018

very low in most solvents, the use of high-sensitivity detectors allows the determination of τ with great precision. The generation of $^1O_2$ can also be detected indirectly by the triplet state decay of β-carotene. However, these time-resolved measurements require highly sophisticated and expensive equipment, which makes the dissemination of the use of these techniques difficult [7].

Measurements at steady state have been widely employed as an alternative method for the oxidation of specific substrates (chemical trap) that readily react with singlet oxygen, among the compounds used as $^1O_2$ trap as 1,3-diphenylisobenzofuran, tryptophan, p-nitrosodimethylaniline acid, anthracene-9,10-dipropionic acid, benzotriazole, betacyanin, bovine serum albumin and uric acid. This indirect method is based on the quantitative analysis of substrate photo-oxidation reactions, determined by the $^1O_2$ consumption method, during the PS photo-excitation. The substrate concentration decay can be directly related to the amount of generated singlet oxygen. In this way, uric acid (UA), an antioxidant compound present in the human body, is a suitable chemical trap for singlet oxygen [8] and has been used as an evaluator of photodynamic activity of potential photosensitizers in PDT [9]. The reaction of photo-oxidation of uric acid via $^1O_2$ may lead to the formation of products such as triuret, allantoxaidin, oxanate ion, and carbon dioxide [10]. However, all the mentioned indirect methods based on chemical trapping require the PS illumination for a specific period of time. The consumption of the substrates allows for the calculations of Φ_Δ. However the usual calculation methodology is applied only to photo-stable PS. For the PS that undergoes the photobleaching process, the photons actually absorbed diminish during the irradiation procedures due to PS concentration decreases.

In the present study, UA was used as a chemical trap for the indirect determination of singlet oxygen quantum yield using a polychromatic LED light source, while considering PS photobleaching in the methodology.

This new methodology was applied to compounds from the classes of chlorophyll (CD) and xanthene derivatives (XD), which have been studied as potential photosensitizers in PDT [11–15]. CD exhibit two main characteristic bands: the Soret band (400 nm region) and the Q-band (660 nm region); the latter is within a region of interest in PDT, called a photo-therapeutic window (600–800 nm) due to the deeper penetration of light into biological tissues [16]. XD have a characteristic absorption band in the region from 450 to 550 nm that can undergo red-shift displacement upon hydrogen substitution by halogens in their xanthene core [17].

2. Materials and methods

2.1. Chemicals

The chlorophyll derivatives used in the present work were magnesium chlorophyll (Mg-Chl), zinc chlorophyll (Zn-Chl), copper chlorophyll (Cu-Chl), pheophytin (Pheo), pheophorbide (Pheid), and zinc chlorophyllide (Zn-Chld), all in ethanol solutions. The xanthene derivatives utilized were fluorescein (FSC), N-fluorescein (N-FSC), eosin Y (EOS), erytrosin B (ERI), and rose bengal B (RBB), all in aqueous buffer solutions. All structures are illustrated in Fig. 1.

Chlorophyll Derivatives (CD): Mg-Chl was extracted from spinach according to the description of Svec [18]. Other derivatives were synthesized from Mg-Chl following the procedures described in the literature [19–22]. The CD were purified using thin layer circular chromatography – Chromatotron (Harrison Research, model 8924) with silica as a stationary phase and characterized by electronic spectra in the visible region (Varian UV-Vis spectrophotometer, model Cary 50) and ^{1}H NMR (Varian, Gemini 300 MHz). DMSO stock solutions of CD ($\sim 10^{-3}$ mol L^{-1}), standardized by UV–vis. These derivatives were prepared and frozen stored in the dark in order to avoid photodegradation [20,22,23]. The working solutions contained less than 1% of DMSO (v/v), which did not influence the final results.

Xanthene Derivatives (XD): fluorescein (FSC, Carlo Erba), eosin Y (EOS, Reagen), erythrosin B (ERI, Vetec), and rose bengal B (RBB, Nuclear) exhibited high purity, as demonstrated by ^{1}H NMR analysis. Besides these dyes, we synthesized 2-(3,6-dihydroxy-9-acridinyl) benzoic acid, known as azafluorescein (N-FSC), using a methodology adapted from the literature [24]. DMSO stock solutions of N-FSC ($\sim 10^{-3}$ mol L^{-1}) standardized by UV–vis were prepared and stored frozen in the dark. The working solutions contained less than 1% of DMSO (v/v), which did not influence the final results. All other XD stock solutions were prepared in water, kept in the dark, and stored below 0 °C.

Uric acid, zinc, and copper acetates were purchased from Sigma–Aldrich (WGK, Germany). All solvents and reagents were of analytical grade and used without previous purification.

2.2. LED emission spectrum measurements

The LED emission spectra were measured in a Varian-Cary Eclipse spectrofluorometer. For CD, the LED light source was made with a diode array system containing 6 LED units with maximum emission at 663 nm (EverLight Co., Taiwan, 5.0 mW/LED measured by a Handheld Laser Power Meter/Edmund Optics Inc., USA). For XD, the LED units (Sun LED Co., USA) had maximum emission at 505 nm (7.6 mW/LED, applied to FSC and N-FSC) and at 520 nm (2.1 mW/LED, applied to EOS, ERI, and RBB). The individual potencies of the described LED corresponded to the total light emission/LED.

2.3. Uric acid (UA) test

In a typical experiment, 3.0 mL of air-saturated solutions were used. For CD dyes, ethanol was utilized as a solvent, while for XD dyes, an aqueous phosphate buffer (Na_2HPO_4, 7.5 mmol L^{-1} at pH 7.25) was used. The solutions were prepared with UA at fixed concentration (1.0×10^{-4} mol L^{-1}) and each PS at three different concentrations (1, 2, and 5 μmol L^{-1}). Samples were added to cuvettes with 1.00 cm of path length and four quartz faces, under air bubbling due to the action of an air compressor (Big Air, Super Pump A320). The PS was illuminated by a set of six LED units coupled to a home-made cuvette holder for the Varian UV-Vis spectrophotometer, model Cary 50. This equipment works in phase-radiation mode, in which incident external light does not cause interferences. The LED illumination system of the cuvette holder was positioned at 90° to the spectrophotometer beam, which permitted simultaneous, spectrophotometric determination and irradiation.

The sample absorption spectra (250–800 nm) were recorded using a UV-Vis spectrophotometer (scanning kinetic mode). The samples (PS plus UA) were irradiated in the visible region and monitored for up to 400 min, and the $^1O_2$ scavenger absorption was monitored through a decrease in the electronic absorption band of UA for CD in ethanol, and for XD in aqueous buffer solutions, both at around 293 nm. While the UA peak was monitored as a function of time, the photodegradation of CD and XD was accomplished. CD photobleaching was monitored at the Q-bands at λ_{max} = 663 nm (Mg-Chl), 667 nm (Pheo and Pheid), 650 nm (Cu-Chl), and 657 nm (Zn-Chl and Zn-Chld). The XD photobleaching was followed at λ_{max} = 491 nm (FSC and N-FSC), 517 nm (EOS), 525 nm (ERI), and 543 nm (RBB). Therefore, the kinetics of UA oxidation was determined concurrently with the photodegradation of PS derivatives in the same assay.

(A)

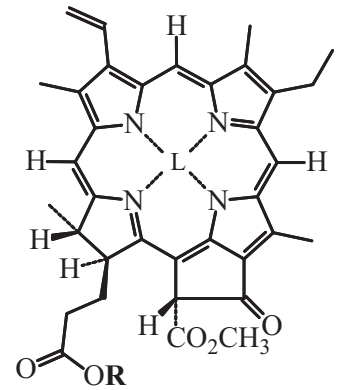

Chls	Ligand (L)	Residue (R)
Mg-Chl	Mg	Phytyl
Zn-Chl	Zn	Phytyl
Cu-Chl	Cu	Phytyl
Pheo	2H	Phytyl
Pheid	2H	H
Zn-Chld	Zn	H

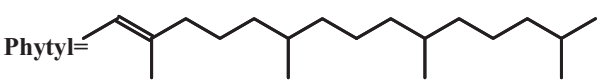

(B)

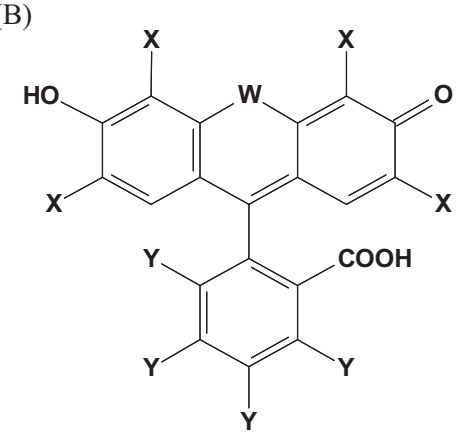

XD	X	Y	W
FSC	H	H	O
N-FSC	H	H	N
EOS	Br	H	O
ERI	I	H	O
RBB	I	Cl	O

Fig. 1. Molecular structure of chlorophyll and xanthene derivatives.

The decrease in the scavenger substrate (UA) absorbance was fitted using a bi-exponential model (Eq. (1)), therefore providing two decay rate constants k_1 and k_2:

$$A = A_0 + B_1 e^{-k_1 t} + B_2 e^{-k_2 t} \quad (1)$$

B_1 and B_2 are the amplitude decays of the UA absorption within the first and second stages, respectively; t is the irradiation time; k_1 and k_2 are the substrate photodegradation rate constants; and A is the absorbance (UV region). Furthermore, the kinetics of concurrent PS photobleaching was evaluated using single mono-exponential decay:

$$A = A'_0 + Be^{-k_{PB}t} \quad (2)$$

where B is the amplitude decay of PS absorbance and k_{PB} is the photobleaching rate constant.

3. Theory/calculation

3.1. Theory

Fisher et al. [9] presented a first empirical methodology for the determination of photodynamic activity or a relative photodynamic scale (PA) of photosensitizers employing a LASER light source. This proposition based on UA as a chemical probe for $^1O_2$ scavenger is represented as Eq. (3).

$$PA = \frac{\Delta A_{UA} 10^5}{E_0 t A_{PS}(\lambda_{irr})} \quad (3)$$

where ΔA_{UA} is the decrease in absorbance at 293 nm, E_0 is the fluency rate (W/m), t is the irradiation time (s), $A_{PS}(\lambda_{irr})$ is the PS absorbance at the monochromatic wavelength radiation, and the term 10^5 is a correction factor. The photodynamic scale empirically proposed [9] in Eq. (3) can be deduced as follows: the amount of photons emitted by the monochromatic source is calculated. Since the energy of a photon is $h\nu$, the number of emitted photons (N_{Em}) corresponds to the total energy (E):

$$N_{Em} = \frac{E}{h\nu} \quad (4)$$

where ν is the radiation frequency and h is the Planck constant ($h = 6.626 \times 10^{-34}$ J s). However, the energy is given by the product of the power (P, in mW) in the time interval (Δt) of emission of the source ($E = P\Delta t$) and ($\nu Y = c/\lambda$, c: light velocity in vacuum ($c = 2.997 \times 10^8$ m s^{-1})). Thus, we obtain Eq. (5) [25]

$$N_{Em} = \frac{\lambda P \Delta t}{hcN_a} \quad (5)$$

where N_a is Avogadro's constant ($N_a = 6.022 \times 10^{23}$ mol^{-1}).

According to the Grotthus–Draper law, only the absorbed light during a photochemical process may cause chemical changes [26]; therefore, it is necessary to evaluate properly the amount of photons (N) absorbed by the PS at the given wavelength, which can be estimated in an approximate way by multiplying N_{Em} and $A_{PS}(\lambda_{irr})$ [27].

To express the efficiency (γ) of a photochemical reaction, the quantum yield (ϕ) is defined as the number of molecules formed or

decomposed (n_{reac}) in relation to the amount of photons absorbed during the process (Eq. (6)) [26].

$$\phi = \frac{n_{reac}}{N} \tag{6}$$

Thus, the amount of $^1O_2$ generated is proportional to the UA substrate oxidation, and the decomposition of this substrate can be monitored, for instance, by its absorption decreases while the PS is illuminated, which is based on Eq. (7). Moreover, the PA value is proportional to the Φ_Δ:

$$PA = \frac{\Delta A_{UA} N_a hc}{\lambda P \Delta t A_{PS}(\lambda_{irr})} \tag{7}$$

For a LASER device emitting at $\lambda = 660$ nm, the product of the constants provides the factor 10^5, leading to Eq. (8). This equation is comparable to Eq. (3), as proposed by Fischer et al. [9].

$$PA = \frac{\Delta A_{UA} 10^5}{P \Delta t A_{PS}(\lambda_{irr})} \tag{8}$$

However, instead of the PA (photodynamic activity or photodynamic scale), it is more interesting to evaluate the quantum yield of singlet oxygen, the values of which can be directly compared with literature data.

3.2. Chemical photodynamic efficiency (γ_Δ) and the quantum yield of singlet oxygen (Φ_Δ)

The photodynamic activity scale (PA) proposed by Fisher is only suitable for monochromatic sources and it does not include the determination of Φ_Δ. Bonacin et al. [27] proposed a mathematical treatment that permits evaluating the Φ_Δ from PA values using standard references. Additionally, they proposed the quantification of the number of photons using polychromatic radiation. They consider the total emission spectrum of the source, since the emitted radiation occurs with significant intensities at several wavelengths.

Thus, the number of photons emitted by a polychromatic source in a specified period of time Δt is determined by analyzing the emission at each wavelength, i.e., Eq. (5) integrated in the range λ_1–λ_2 results in Eq. (9), where $P_{(\lambda)}$ represents the potency at each wavelength.

$$N_{Em} = \frac{\Delta t}{hcN_a} \int_{\lambda_1}^{\lambda_2} P_{(\lambda)} d\lambda \tag{9}$$

Simultaneously, the total number of photons emitted does not correspond to the total absorbed light. Thus, it is necessary to consider the actual fraction of light from the incident light absorbed by the PS at each wavelength. This fraction or absorption ratio of a chromophore is given by the Lambert-beer law ($A = \varepsilon bc$). Considering that the absorbance is given by $\log(I_0/I)$, the intensity of light absorbed by the system (I_a) is calculated by Eq. (10).

$$I_a = I_0(1 - 10^{-bc\varepsilon}) \tag{10}$$

Therefore, the amount of photons absorbed by a PS irradiated by a polychromatic array is obtained through Eq. (11), which relates the capability of the emission source at each wavelength, in power, to the ability to absorb light of the PS at the same wavelength [27].

$$N_{Abs} = \frac{\Delta t}{N_a hc} \int_{\lambda_1}^{\lambda_2} I_{0(\lambda)}(1 - 10^{-bc\varepsilon(\lambda)}) P_{(\lambda)} d\lambda \tag{11}$$

Eq. (11) is true for photostable compounds, but for PS that undergo photobleaching, the continuous decrease in light absorption capacity must be considered. Therefore, the dosimetric quantification of $^1O_2$ using this methodology needs adjustments. For this, the influence of the decrease in [PS] was included in Eq. (11) by adding the term $e^{-k_{PB}t}$, which corrects the absorbed light intensity (Eq. (12)). This term comes from the kinetic model of photobleaching reactions of PS, which usually obey monoexponential profiles over time [28].

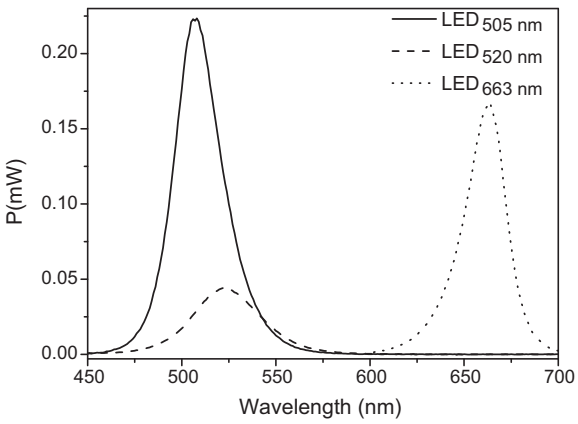

Fig. 2. Emission spectra of LED systems utilized in the irradiation experiments.

$$N_{Abs} = \frac{1}{N_a hc} \int_0^t \int_{\lambda_1}^{\lambda_2} P_{(\lambda)} I_0 (1 - 10^{-bc\varepsilon}) e^{-k_{PB}t} d\lambda dt \tag{12}$$

Therefore, the proposed Eq. (12) permits calculating the amount of photons absorbed by a PS for dyes that decompose during irradiation. Furthermore, this equation allows estimating the efficiency (γ) of the process involving photochemical reactions of stable and unstable PS against light. For stable compounds, the term k_{PB} tends to zero; thus, Eq. (12) turns back into Eq. (11).

The chemical photodynamic efficiency (γ_Δ) was estimated by Eq. (13) [29].

$$\gamma_\Delta \propto \frac{k_1}{N_{Abs}} \tag{13}$$

Finally, the quantum yield of singlet oxygen (Φ_Δ) was calculated using Eq. (14):

$$\phi_\Delta = \frac{\phi_\Delta^S}{\gamma_\Delta^S} \gamma_\Delta \tag{14}$$

4. Results and discussion

The molar absorptivity of the chromophores and the intensity of emission of the light sources are both dependent on the wavelength. For efficient photochemical reactions, it is very important to match PS absorption with light emission spectra for higher photon absorption yield [26]. The absorption maxima and molar absorptivity coefficients of both classes of PS used in the present work are presented in Table 1.

The LED employed in the experiments with all CD emits red light radiation with a maximum at 663 nm ($LED_{663\,nm}$), whereas for xanthenes (XD) two different green light LED ($LED_{505\,nm}$ and $LED_{520\,nm}$) were used. Their emission spectra are illustrated in Fig. 2. These three LED units were utilized in such a way as to assure a maximum overlap between the LED emissions and the PS absorption spectra.

Instead of using Eq. (8), whose experimental methodology imposes monochromatic light and ΔA_{UA} for a specified period of time (Fisher et al. [9]), we followed the methodology and calculation based on Eq. (12), which permits determining N_{Abs} during

Table 1
Wavelengths of maximum absorption (λ_{abs}), and molar absorption coefficient (ε) of CD in ethanol and XD in aqueous phosphate buffer at 25 °C.

Chlorophylls			Xanthenes		
	$\lambda_{max,Qband}$ (nm)	ε (10^3 L mol^{-1} cm^{-1})		λ_{max} (nm)	ε (10^3 L mol^{-1} cm^{-1})
Mg-Chl	665	80.1	FSC	491	76.9
Pheo	667	66.7	N-FSC	491	76.7
Zn-Chl	659	82.0	EOS	517	96.6
Cu-Chl	650	56.3	ERI	525	96.0
Pheid	667	49.0	RBB	543	111.0
Zn-Chld	660	75.3			

a period of time of illumination considering the spectral overlap among the polychromatic light source and the PS absorption, as well as the PS photobleaching reaction. The chemical photodynamic efficiency (γ_Δ) and the quantum yield (Φ_Δ) of the singlet oxygen were determined based on Eqs. (13) and (14), respectively.

4.1. UA oxidation and PS photobleaching

One advantage of UA as a chemical dosimeter of singlet oxygen is its electronic absorption, which occurs in the UV region ($\lambda < 350$ nm), with a maximum at ca. 293 nm (in ethanol and in aqueous phosphate buffer). Both classes of compounds, CD and XD derivatives, were excited at the electronic visible light region without direct photo-excitation of the UA. Thus, the restricted spectral overlap between the UA substrate and the PS absorption was helpful in the system analysis.

Once the photosensitizers are excited to ^{1}PS, one fraction of these molecules undergoes intersystem crossing (ISC) and reaches the triplet state (^{3}PS), which transfers energy to molecular oxygen in solution forming $^1O_2$, which in turn reacts with the uric acid molecule. The process of UA oxidation by photo-excitation of the PS can be observed in Fig. 3 for Mg-Chl and RBB as examples.

As illustrated in Fig. 3, UA degradation was observed simultaneously with PS photobleaching upon irradiation, as demonstrated through the absorbance decays of the main bands. For the UA degradation, Eq. (8) is employed, using the term ΔA_{UA} that is related to the change of absorbance at 293 nm before and after the PS irradiation time [9,30]. However, the definition of the reaction time is quite difficult to specify when two different systems are compared, such as, in our case, CD and XD classes of dyes. Therefore, the degradation rate constant of the UA was utilized, instead of ΔA_{UA}, as proposed earlier by Bonacin et al. [27], who first employed red beetroot extract as a chemical probe instead of UA. In the mentioned paper, the oxidation reaction of the substrate followed a first-order kinetic law.

However, the UA absorbance variations at 315 nm (inserts in Fig. 3) clearly demonstrated the existence of a first step, in which an UA-intermediate product was formed (<30 min), and also of a second slower step (>30 min), in which such species were subsequently consumed [31]. This consecutive reaction can also be noticed in the UA absorbance at 293 nm (Fig. 3). In fact, for all photosensitizers investigated, the UA absorption (293 nm), which decreases as a function of time, did not adjust with either first-order or second-order kinetic laws. Nevertheless, the data points presented a curve fitting to a first-order kinetic model, considering two consecutive steps. Among all investigated PS, only Cu-Chl did not exhibit two reaction steps unequivocally; this PS showed data that fit the first-order equation.

The rate constants evaluated from the UA oxidation curves are presented in Table 2 for each PS at three concentrations. It can be observed that the first rate constant (k_1) was nearly directly dependent on PS concentration, while the k_2 exhibited a concentration-independent effect. The mechanism of UA oxidation is well known [32]; singlet oxygen acts in a first stage of degradation related to the oxidation of the UA, which leads to the intermediate formation [31].

In fact, in additional experiments using XD (not shown), the illumination was interrupted at 30 min (time roughly related to the first stage of UA reaction), and even in the dark, the UA degradation process still continued. The k_2 values obtained with samples in the absence of irradiation were comparable to those of samples submitted to continuous light irradiation. These results indicate that this second step is related to the instability of the formed intermediate, which justifies the light and concentration effect independent of k_2. These results confirm the importance of PS photosensitization only in the first stage and that k_2 is not relevant for the

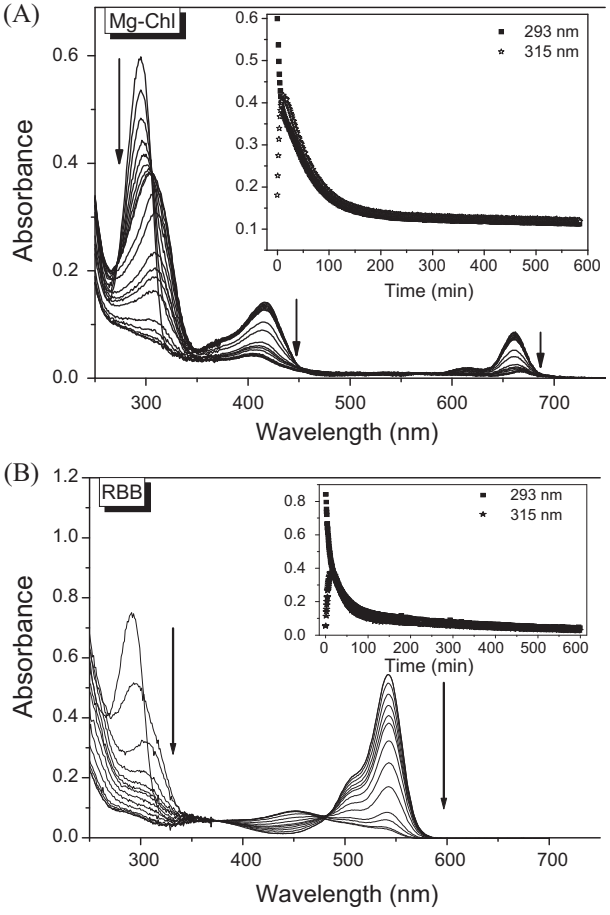

Fig. 3. Spectral variations of the [PS] ~10^{-6} mol L^{-1} in the presence of [UA] = 1.0×10^{-4} mol L^{-1} with illumination: (A) Mg-Chl in ethanol and (B) RBB in aqueous buffer solution. The arrows show the absorbance behavior during irradiation. The inset shows UA absorbance variations at 293 and 315 nm as a function of time. T = 25 °C.

Table 2
Rate constants from UA degradation (k_1 and k_2) and PS photobleaching (k_{PB}). CD in ethanol and XD in aqueous phosphate buffer at 25 °C.

	PS (μmol L^{-1})	k_1 (10^{-3} s^{-1})	k_2 (10^{-3} s^{-1})	k_{PB} (10^{-5} s^{-1})
Mg-Chl	1	1.11	0.10	14.7
	2	2.14	0.11	13.8
	5	4.61	0.11	15.0
Pheo	1	0.58	0.10	–
	2	1.32	0.12	–
	5	3.14	0.20	–
Zn-Chl	1	1.81	0.14	2.16
	2	3.96	0.20	3.74
	5	8.46	0.21	2.57
Cu-Chl	2	0.07	–	–
	4	0.09	–	–
	5	0.12	–	–
Pheid	1	0.86	0.10	–
	2	2.13	0.13	–
	5	4.19	0.19	–
Zn-Chld	1	1.24	0.11	3.01
	2	2.40	0.13	3.62
	5	4.52	0.17	3.03
FSC	1	0.17	0.08	10.2
	2	0.30	0.19	11.9
	5	0.40	0.37	14.9
N-FSC	1	0.23	0.09	10.1
	2	0.30	0.20	14.7
	5	0.64	0.30	18.4
EOS	1	0.58	0.20	6.83
	2	1.14	0.39	8.43
	5	3.09	0.71	9.97
ERI	1	0.71	0.57	14.0
	2	1.50	0.58	17.0
	3	3.47	0.74	20.8
RBB	1	0.91	0.58	8.68
	2	2.49	0.64	8.37
	5	4.92	0.42	6.17

determination of Φ_Δ. In addition, we estimated the isolated kinetic curve of UA at 292 nm by subtracting the kinetic intermediate in the same wavelength, resulting in a profile of first-order exponential decay. The rate constant values of AU degradation found with this method showed no significant differences using an exponential fitting model with two consecutive steps (adopted throughout this work). This is because the rate constants of second stage are much smaller than the first step, so that the interference caused by second step the values of k_1 is very small. Moreover, it is worth of mention that the constants k_1 evaluated from UA oxidation curves in the presence of several PS, and which were further corrected considering the influence of possible cross-talk in the system, i.e. contamination of the absorbance at the chosen (analytical) wavelength from other spectral components, has been ruled out (see Supplementary data).

Except for Pheo, Pheid, and Cu-Chl, which present relatively higher photostability, all other analyzed PS underwent photobleaching in experiments with the presence of UA (illustrated in Fig. 3). The rate constants of photobleaching (k_{PB}) obtained from curve fittings of experimental points of the PS photobleaching using the first order exponential decay law are also presented in Table 2; these constants were two orders of magnitude smaller than k_1.

For XD, the photobleaching can be related to the presence of singlet oxygen generated in situ, since this reaction was significantly reduced in experiments with XD in aqueous solution purged with N_2 (not shown).

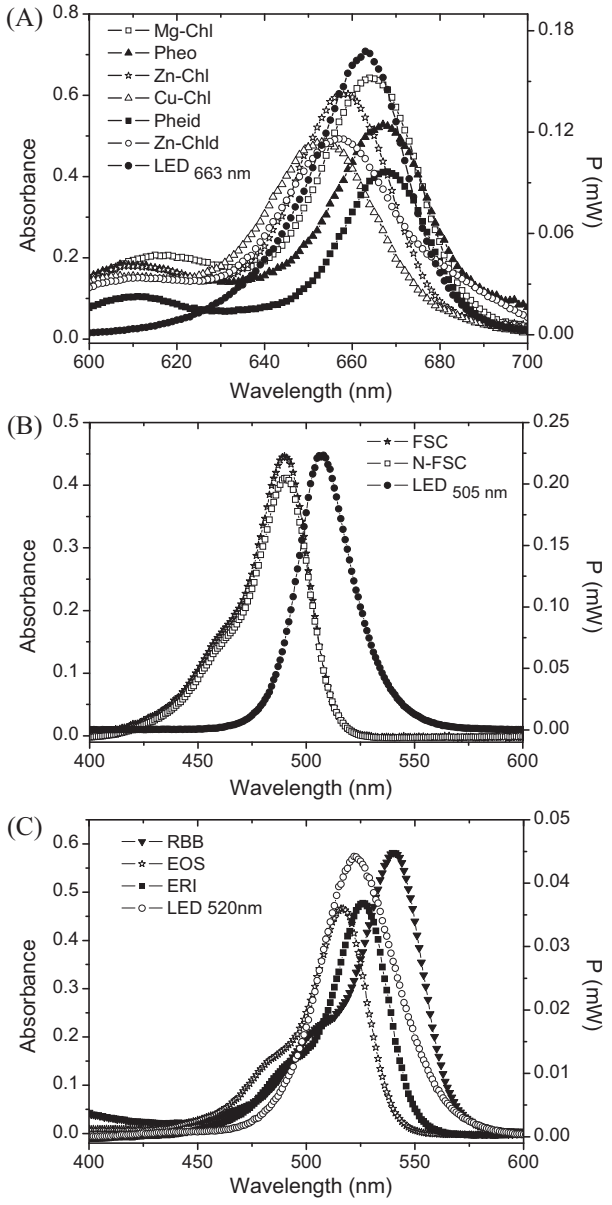

Fig. 4. PS absorption spectra (at 5 μM) and the LED emission spectra (mW): (A) CD, (B) FSC and N-FSC, and (C) RBB, EOS, and ERI.

4.2. Time-dependence of photon absorption and PS photobleaching

Fig. 4 displays the emission spectra of the chosen LED system (in mW) plus the absorption spectra of the corresponding photosensitizers, CD (Fig. 4A) and XD (Fig. 4B and C) at 5 μmol L^{-1}. The LED light utilized for all CD emits in the range of 600–700 nm ($LED_{663\,nm}$) (Fig. 4A). For FSC and N-FSC, devices emitting in the range of 440–560 nm with a maximum of emission at 505 nm ($LED_{505\,nm}$) (Fig. 4B), and for EOS, ERI, and RBB, a device emitting at 480–580 nm with a maximum at 520 nm ($LED_{520\,nm}$) (Fig. 4C), were employed. The accurate quantification of the overlap is an important requirement for the unequivocal determination of the effectively absorbed photons (N_{Abs}, see Eq. (11)) [33].

In the present work, the PS photostability term is included, since the photobleaching reaction decreases the amount of photons effectively absorbed during the PS irradiation of the sample, and hence, it must be used in the N_{Abs} calculations, resulting in the proposed Eq. (12). In order to compare the calculated amount

Table 3
Number of absorbed photons (N_{Abs}) after 30 and 400 min upon irradiation evaluated for samples containing PS (5 μmol L^{-1}) with and without application of the photobleaching terms. The data in parentheses are the percentage differences between values with and without PB.

PS	$N_{Abs,t=30\,min}$ (10^{-7} mol)		$N_{Abs,t=400\,min}$ (10^{-7} mol)	
	Without PB	PB	Without PB	PB
Mg-Chl	2.01	1.76 (12%)	26.9	7.26 (73%)
Pheo[a]	1.61	1.61	21.5	21.5
Zn-Chl	1.97	1.92 (2.5%)	26.2	19.5 (25%)
Cu-Chl[a]	1.40	1.40	18.6	18.6
Pheid[a]	1.29	1.29	17.2	17.2
Zn-Chld	1.61	1.56 (3.1%)	21.4	15.2 (29%)
FSC	1.84	1.58 (14%)	24.4	6.57 (73%)
N-FSC	1.79	1.50 (16%)	23.9	5.32 (78%)
EOS	0.78	0.71 (9.0%)	10.5	3.96 (62%)
ERI	0.79	0.66 (16%)	10.6	2.12 (80%)
RBB	0.94	0.88 (6.4%)	12.6	6.53 (48%)

[a] No significant photobleaching reaction.

of photons absorbed during the experiments with PB absence and photobleaching, Eq. (12) was applied to the data obtained during 30 and 400 min of irradiation, respectively, using the model without the photobleaching term (Eq. (11)) and the model with the photobleaching term (Eq. (12)). It is worth mentioning that the time values used (30 and 400 min) in the calculations are related respectively to the first (k_1) and second (k_2) stages of UA degradation. The results are presented in Table 3.

The data in brackets in Table 3 show that for 30 min of irradiation without considering photobleaching, up to 16.4% of the photon energy absorption was previously wrongly attributed to the PS photobleaching. For 400 min of irradiation, the PS photodegradation led to a greater error, which reached 80%. The proposed treatment based on Eq. (12) corrects this distortion, because it predicts the real amount of photons absorbed during the irradiation.

4.3. Singlet oxygen quantum yield by uric acid dosimeter

Since only k_1 is relevant in the determination of Φ_Δ, the chemical photodynamic efficiency (γ_Δ) was determined through the data slope (Tables 2 and 3) in Fig. 5, k_1 as a function of N_{Abs}, illustrated for Pheo as an example using Eq. (13).

As observed in Fig. 5, the relationship of k_1 and N_{Abs} is linear as predicted by Eq. (13). This behavior is obtained for all the PS studied. Since γ_Δ was experimentally determined for all compounds, Φ_Δ was calculated (Eq. (14)) for CD and XD using, respectively, Pheid

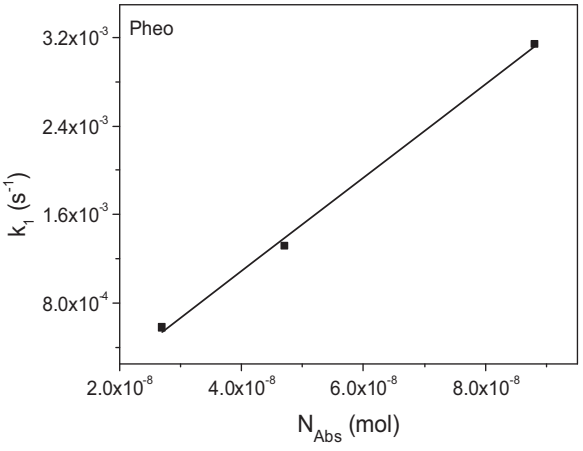

Fig. 5. Observed rate constants (k_1) of UA degradation for Pheo versus the amount of photons absorbed at several [Pheo].

Table 4
Quantum yield (Φ_Δ) of $^1O_2$ calculated for CD and XD. Values from literature and calculated by methods that do not consider (Eq. (11)) and that consider (Eq. (12)) the photobleaching term. CD in ethanol and XD in aqueous phosphate buffer, at 25 °C and Pheid and RBB, used as standards. The data in parentheses are the percentage differences between values with and without PB.

PS	Φ_Δ		Φ_Δ (lit)
	Without PB	PB	
Mg-Chl	0.44	0.47 (6.4%)	0.44[d]
Pheo[a]	0.73	0.73	0.60[e]
Zn-Chl	0.84	0.86 (2.3%)	–
Cu-Chl[a]	0.01	0.01	0[f]
Pheid[a]	0.51[b]	0.51	0.51[b]
Zn-Chld	0.46	0.48 (4.2%)	–
FSC	0.05	0.06 (13.5%)	0.03[g]
N-FSC	0.03	0.03	–
EOS	0.55	0.60 (8.3%)	0.5[g]
ERI	0.52	0.61 (14.8%)	0.6[g]
RBB	0.71[c]	0.75 (5.3%)	0.75[c]

[a] No significant photobleaching reaction.
[b] Used as a standard value for Φ_Δ calculation of CD [43].
[c] Used as a standard value for Φ_Δ calculation of XD [17].
[d] From Ref. [42].
[e] From Ref. [34].
[f] From Ref. [5].
[g] From Ref. [17].

and RBB as standards $\Phi_\Delta{}^s$ [27,34]. The calculated values of γ_Δ and Φ_Δ, presented in Table 4, can be used to compare the efficacy of different photosensitizers.

The Φ_Δ data in Table 4 are discussed taking into account differences in the values calculated by methods that consider the photobleaching term or not: (i) Φ_Δ values are obviously identical for PS that are photostable (Pheo, Pheid, and Cu-Chl); (ii) RBB showed the lowest photobleaching reaction among XD (Table 3 – 7.1 and 48.3% in N_{Abs} for 30 and 400 min, respectively), leading to the lowest difference (5.3% in Φ_Δ); (iii) for CD, the percentage differences in Φ_Δ were found as Mg-Chl > Zn-Chld > Zn-Chl; and (iv) among XD, the differences in Φ_Δ obeyed ERI > N-FSC > FSC > EOS > RBB due to photobleaching. Therefore, the values considering the PS photobleaching in the methodology were up to 15% (ERI) higher than those obtained without considering photobleaching in the calculations.

Therefore, our results showed that the chemical photodynamic efficiency of CD (Table 4) follows the order: Zn-Chl > Pheo > Pheid ≈ Zn-Chld ≈ Mg-Chl » Cu-Chl. The Φ_Δ value determined for Pheo was 1.6 times higher than that of Mg-Chl, the same factor was found in benzene [35]. The largest singlet oxygen quantum yield of Zn-Chl is in agreement with literature data, which show the presence of zinc-coordinated porphyrins as an important factor for Φ_Δ; the observed increase is due to the longer lifetime of the triplet (τ_T) state of these porphyrins [5]. Studies of the dynamics (life time) of the triplet excited state of Mg-Chl, Zn-Chl, and Pheo in acetone performed by Drzewiecka-Matuszek et al. [36] showed that Zn-Chl possesses the highest τ_T in the absence of oxygen, followed by Mg-Chl and Pheo, whereas in the presence of oxygen, the sequence was Mg-Chl, Zn-Chl, and Pheo. In the latter, the τ_T values of Mg-Chl in comparison to Pheo and Zn-Chl are higher in oxygen [36], which can be attributed to a lesser efficiency of energy transfer from the triplet state of Mg-Chl to molecular oxygen than for Zn-Chl and Pheo, justifying the lower Φ_Δ [36]. Additionally, the Φ_Δ value of Zn-Chld, significantly lower than that of Zn-Chl, is due to the conformational changes resulted from complexation between Zn and the propionate group, contributing to the decrease in τ_T [37]. Moreover, porphyrin complexes with copper, a paramagnetic transition metal, have their triplet state lifetime drastically reduced [5], which justifies the low chemical photodynamic efficiency of Cu-Chl.

Regarding XD, the chemical photodynamic efficiency followed the order: RBB > ERI > EOS > FSC ≈ N-FSC (Table 4). FSC and N-FSC, which are very similar in structure, presented low values of Φ_Δ due to the efficient deactivation of the excited singlet to the fundamental ground states ($^*S_1 \rightarrow S_0$) via fluorescence emission ($\Phi_{Fl} = 0.93$, in water) [38,39]. With the increasing number of halogen substituents, a decrease in fluorescence quantum yield Φ_{Fl} is observed, mainly due to the heavy atom effect favoring the intersystem crossing, consequently leading to an increase in singlet oxygen quantum yield [40]. In the case of XD derivatives, this effect is more pronounced when substitution occurs in the xanthene ring, especially in the ortho position relative to the phenolic hydroxyl and quinoidal groups [17,41].

Table 4 also presents the values of singlet oxygen quantum yield of all PS. The values of Φ_Δ found using the present methodology are very similar to literature data determined by traditional methods [34,42,43], which demonstrates the feasibility of the proposed methodology used in the treatment of indirect UA oxidation considering the intrinsic PS photobleaching process.

5. Conclusions

The improved methodology considering the photobleaching of PS can be used as an inexpensive and efficient alternative to evaluate the formation of $^1O_2$ for different photosensitizers (stable and unstable against light) in different systems. We also emphasize in this study the fact that the more precise calculation of the amount of photons absorbed by a system containing a photo-unstable photosensitizer is relevant for the development of methodologies for PDT and PDI dosimetric control.

Acknowledgments

This work was sponsored by the Brazilian funding agencies Fundação Araucária, CNPq and CAPES-NBionet network.

Appendix A. Supplementary data

Supplementary data associated with this article can be found, in the online version, at doi:10.1016/j.jphotochem.2012.01.018.

References

[1] J. Michl, Photophysics of organic molecule in solution, in: M.A. Montalti, L. Credi, M.T. Prodi, Gandolfi (Eds.), Handbook of Photochemistry, 3a ed., Taylor & Francis Group, Boca Raton, 2006, pp. 1–45.
[2] E.D. Sternberg, D. Dolphin, C. Brückner, Porphyrin-based photosensitizers for use in photodynamic therapy, Tetrahedron 54 (1998) 4151–4202.
[3] I.J. Macdonald, T.J. Dougherty, Basic principles of photodynamic therapy, J. Porphyrins Phthalocyan. 5 (2001) 105–129.
[4] E.J. Dennis, D.E. Dolmans, D. Fukumura, R. Jain, Photodynamic therapy for cancer, Nature 3 (2003) 380–387.
[5] M.C. DeRosa, R.J. Crutchley, Photosensitized singlet oxygen and its applications, Coord. Chem. Rev. 233–234 (2002) 351–371.
[6] S.W. Ryter, R.M. Tyrrell, Singlet molecular oxygen ($^1O_2$): a possible effector of eukaryotic gene expression, Free Radical Biol. Med. 24 (1998) 1520–1534.
[7] F.W. Wilkinson, W.P. Helman, A.B. Ross, Quantum yields for the photosensitized formation of the lowest electronically excited singlet state of molecular oxygen in solution, J. Phys. Chem. Ref. Data 22 (1993) 113–262.
[8] B.N. Ames, R. Cathcart, E. Schwiers, P. Hochstein, Uric acid provides an antioxidant defense in humans against oxidant and radical-caused aging and cancer: a hypothesis, Biochemistry 78 (1981) 6858–6862.
[9] F. Fischer, G. Graschew, H.J. Sinn, W. Maier-Borst, W.J. Lorenz, P.M. Schlag, A chemical dosimeter for the determination of the photodynamic activity of photosensitizers, Clin. Chim. Acta 274 (1998) 89–104.
[10] T. Matsuura, I. Saito, Photoinduced reactions – XXI. Photosensitized oxygenation of *N* unsubstituted hydroxypurines, Tetrahedron 24 (1968) 6609–6614.
[11] L.C. Bergstrom, I. Vucenik, I.K. Hagen, S.A. Chernomorsky, R.D. Poretz, In-vitro photocytotoxicity of lysosomotropic immunoliposomes containing pheophorbide *a* with human bladder carcinoma cells, J. Photochem. Pholobiol. B: Biol. 24 (1994) 17–23.
[12] Y.J. Park, W.Y. Lee, B.S. Hahn, M.J. Han, W.I. Yang, B.S. Kim, Chlorophyll derivatives – a new photosensitizer for photodynamic therapy of cancer in mice, Yonsel Med. J 30 (1989) 212–218.
[13] J. Jakus, O. Farkas, Photosensitizers and antioxidants: a way to new drugs, Photochem. Photobiol. Sci. 4 (2005) 694–698.
[14] W.T. Li, H.W. Tsao, Y.Y. Chen, S.W. Cheng, Y.C. Hsu, A study on the photodynamic properties of chlorophyll derivatives using human hepatocellular carcinoma cells, Photochem. Photobiol. Sci. 6 (2007) 1341–1348.
[15] F. Stracke, M. Heupel, E. Thiel, Singlet molecular oxygen photosensitized by Rhodamine dyes: correlation with photophysical properties of the sensitizers, J. Photochem. Photobiol. A: Chem. 126 (1999) 51–58.
[16] F.I. Simplicio, F. Maionchi, N. Hioka, Terapia Fotodinâmica: Aspectos Farmacológicos: Aplicações e Avanços Recentes no Desenvolvimento de Medicamentos, Quim. Nova 25 (2002) 801–807.
[17] E. Gandin, Y. Lion, A. Van de Vorst, Quantum yield of singlet oxygen production by xanthene derivatives, Photochem. Photobiol. 37 (1983) 271–278.
[18] W.A. Svec, The isolation, preparation, characterization, and estimation of the chlorophylls and the bacteriochlorophylls, in: D. Dolphin (Ed.), The Porphyrins, Physical Chemistry. Part C, vol. V, Academic Press, New York, 1978, pp. 342–394.
[19] P.H. Hynninen, S. Lotjomen, Preparation of phorbin derivates from chorophyll mixture utilizing of selective hydrolysis, Communications (1980) 539–541.
[20] M.R. Wasielewski, W.A. Svec, Synthesis of covalently linked dimeric derivatives of chlorophyll a, pyrochlorophyll, chlorophyll b, and bacteriochlorophyll a, J. Org. Chem. 45 (1980) 1969–1974.
[21] Y. Nonomura, S. Igarashi, N. Yoshioka, H. Inoue, Spectroscopic properties of chlorophylls and their derivatives, Influence of molecular structure on the electronic state, Chem. Phys. 220 (1997) 155–166.
[22] H. Kupper, M. Spiller, F.C. Küpper, Photometric method for the quantification of chlorophylls and their derivatives in complex mixtures: fitting with Gauss-peak spectra, Anal. Biochem. 286 (2000) 247–256.
[23] D. Dolphin, The Porphyrins, Physical Chemistry, Part A, vol. III, Academic Press Inc., New York, 1978, 463pp.
[24] D.V. Samoilov, V.P. Martynova, A.V. El'tsov, Nitro derivatives of fluorescein, Russ. J. Gen. Chem. 69 (1999) 1450–1460.
[25] P. Atkins, J. Paula, Physical Chemistry, 8a ed., Oxford Press, New York, 2006.
[26] K.K. Rohatgi-Mukherjee, Fundamentals of Photochemistry, Wiley, New York, 1978.
[27] J.A. Bonacin, F.M. Engelmann, D. Severino, H.E. Toma, M.S. Baptista, Singlet oxygen quantum yields (Φ_Δ) in water using beetroot extract and an array of LEDs, J. Braz. Chem. Soc. 20 (2009) 31–36.
[28] H.H. Tonnesen, Photostability of Drugs and Drug Formulations, 2nd ed., CRC Press, Washington, 2004.
[29] M. Montalti, A. Credi, L. Prodi, M.T. Gandolfi, Handbook of Photochemistry, 3a Ed., Taylor & Francis Group, Boca Raton, 2006, 601–615.
[30] A.P.J. Maestrin, A.C. Tedesco, C.R. Neri, M.E.F. Gandini, O.A. Serra, Y. Iamamoto, Synthesis, spectroscopy and photosensitizing properties of hydroxynitrophenylporphyrins, J. Braz. Chem. Soc. 15 (2004) 708–713.
[31] K. Kahn, P.A. Tipton, Spectroscopic characterization of intermediates in the urate oxidase reaction, Biochemistry 37 (1998) 11651–11659.
[32] M.V. George, V. Bhat, Photooxygenations of nitrogen heterocycles, Chem. Rev. 79 (1979) 447–478.
[33] M. Hoebeke, X. Damoiseau, Determination of the singlet oxygen quantum yield of bacteriochlorin *a*: a comparative study in phosphate buffer and aqueous dispersion of dimiristoyl-L-α-phosphatidylcholine liposomes, Photochem. Photobiol. Sci. 1 (2002) 283–287.
[34] A.A. Krasnovsky, K.V. Neverov, S. Egorov, B. Roeder, T. Levald, Photophysical studies of pheophorbide *a* and pheophytin *a*. Phosphorescence and photosensitized singlet oxygen luminescence, J. Photochem. Photobiol. B: Biol. 5 (1990) 245–254.
[35] C. Tanielian, C. Wolff, Porphyrin-sensitized generation of singlet molecular oxygen: comparison of steady-state and time-resolved methods, J. Phys. Chem. 99 (1995) 9825–9830.
[36] A. Drzewiecka-Matuszek, A. Skalna, A. Karocki, G. Stochel, L. Fiedor, Effects of heavy central metal on the ground and excited states of chlorophyll, J. Biol. Inorg. Chem. 10 (2005) 453–462.
[37] R. Angerhofer, Chlorophyll triplets and radical pairs, in: H. Scherr (Ed.), Chlorophylls, CRC Press, Boca Raton–Ann Arbor, London, 1991, p. 945.
[38] R. Sjöback, J. Nygren, M. Kubista, Absorption and fluorescence properties of fluorescein, Spectrochim. Acta A 51 (1995) 7–21.
[39] J. Slavik, Fluorescent Probes in Cellular and Molecular Biology, CRC Press, Boca Raton, 1994.
[40] R.J. Lakovicz, Principles of Fluorescence Spectroscopy, 2 ed., Plenum, New York, 1999.
[41] D.C. Neckers, R. Bengal, J. Photochem. Photobiol. A 47 (1989) 1–29.
[42] R.W. Redmond, J.N. Gamlim, A complilation of singlet oxygen yields from biologically relevant molecules, Photochem. Photobiol. 70 (1999) 391–475.
[43] B. Roeder, D. Naether, T. Lewald, M. Braune, C. Nowak, W. Freyer, Photophysical properties and photodynamic activity in vivo of some tetrapyrroles, Biophys. Chem. 35 (1990) 303–312.